Accepted in Precision Engineering on 10/5/2020

Volume 65, September 2020, pp. 64-71; 10.1016/j.precisioneng.2020.05.004

Elastic recovery of monocrystalline silicon during ultra-fine rotational grinding

Ning Huang[1], Ying Yan[1], Ping Zhou[1*], Renke Kang[1], Dongming Guo[1] and Saurav Goel[2,3]

[1]Key Laboratory for Precision and Non-traditional Machining Technology of Ministry of Education, Dalian University of Technology, Dalian 116024, China

[2] School of Engineering, London South Bank University, 103 Borough Road, London SE1 0AA, UK

[3] School of Aerospace, Transport and Manufacturing, Cranfield University, Bedfordshire, MK43 0AL, UK

Abstract

Micromachining of brittle materials like monocrystalline silicon to obtain deterministic surface topography is a 21st Century challenge. As the scale of machining has shrunk down to sub-micrometre dimensions, the undulations in the machined topography start to overlap with the extent of elastic recovery (spring back) of the workpiece, posing challenges in the accurate estimation of the material's elastic recovery effect. The quantification of elastic recovery is rather complex in the grinding operation due to (i) randomness in the engagement of various grit sizes with the workpiece as well as (ii) the high strain rate employed during grinding as opposed to single grit scratch tests employed in the past at low strain rates. Here in this work, a method employing inclination of workpiece surface was proposed to quantify elastic recovery of silicon in ultra-fine rotational grinding. The method uniquely enables experimental extraction of the elastic recovery and tip radius of the grits actively engaged with the workpiece at the end of the ultra-fine grinding operation. The proposed experimental method paves the way to enable

* Corresponding author, email: pzhou@dlut.edu.cn

a number of experimental and simulation endeavours to develop more accurate material constitutive models and grinding models targeted towards precision processing of materials. It can also be shown that using this method if the tip radius distribution of active grits is measured at different time instances, then this data can be used to assess the state of the grinding wheel to monitor its wear rate which will be a useful testbed to create a digital twin in the general framework of digital manufacturing processes.

Keywords: Brittle materials; rotational grinding; silicon; elastic recovery; grit tip radius

Abbreviations

h_e	:	Recovery depth
h_f	:	Residual depth
h	:	Penetration depth
α	:	Coefficient depending on material and geometry
k	:	Coefficient depending on cutting velocity
C	:	Function of α and k
ERR:		Elastic recovery ratio (h_e/h)
TTV:		Total thickness variation

1. Introduction

Monocrystalline silicon finds numerous electronic applications due to its excellent properties such as high hardness, good thermal, chemical stability, and large bandgap appropriate to be used in the semiconductor industry. Driven by the need for miniaturization, strenuous efforts are in place to adhere to Moore's Law (which says that the count of transistors on a silicon chip doubles every two years) which poses a

challenging requirement for fabricating ultra-thin silicon wafers (~100 μm thickness) with deterministic precision [1]. Furthermore, as per the International Technology Roadmap for Photovoltaics [2], the quality factors affecting yield and costs are total thickness variation (TTV), surface quality (variations (roughness) and uniformity) and strength of the wafer (number of defects).

Ultra-fine rotational grinding is one of the efficient techniques for fabrication of optical quality (a root-mean-squares figure accuracy $< \lambda/10$ with $\lambda < 1$ μm) surfaces in a wide range of brittle materials including silicon [3]. In the past, the concept of machining brittle materials in the ductile-mode such that the material removal occurs by virtue of plastic deformation as opposed to fracture has been well demonstrated in materials ranging from germanium, silicon and silicon carbide [4-5]. For this reason, various theoretical models are proposed aimed at optimisation of the rotational grinding process [6-7]. These models have shown that the quality of the finish depends on grinding parameters, grinding wheel topography, and stability of the tool-workpiece contact (chatter, vibrations etc.). Besides these factors, another important factor that leads to deviations from the envisioned programmable parameters compared to the experimental measurements is inherent to the material itself, which includes, for example, residual stresses and elastic recovery of the material that occurs upon release of the cutting load exerted by the moving cutting tool.

However, it is worth noting that few reported techniques describe the characterisation and measurement of the tip radius distribution of actively engaged grits and the material elastic recovery in ultra-fine rotational grinding up to now. To fill these gaps, a novel method of grinding on an inclined surface was developed to quantify the extent of elastic recovery of silicon as well as the tip radius distribution of grinding grits. To our best knowledge, this is the first paper elucidating the elastic recovery of monocrystalline

silicon under the realistic experimental rotational grinding conditions. Likewise, the idea of being able to monitor the wear of grinding grits with time dependency to align the grinding process to digital micromanufacturing is being coined for the first time. It is anticipated that this investigation will have many practical applications in researches on ultra-fine grinding prediction and optimisation.

2. Literature review

As shown in Fig. 1, most of the research on grinding considers grit tip radius to be equivalent to an imaginary spheroidal shape radius of the grit and assumes rigid-plastic material while revealing the effect of the grinding process and wheel parameters on average attainable depth-of-cut [8-9].

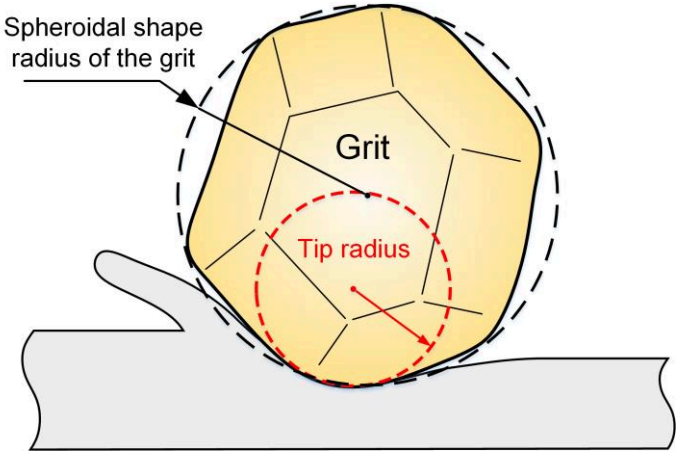

Fig. 1. Illustration of the imaginary spheroidal shape tip radius of a grinding grit.

Earlier, Zhou et al. [7] proposed a novel model of ultra-fine rotational grinding incorporating elastic-plastic response of the material and grit tip radius by adding two coefficients relating to material's elastic recovery and grit tip radius respectively. Their results show that the simplified assumption of assuming the grit tip radius as equal to the average grit radius becomes unreasonable in ultra-fine grinding.

However, in their work, they did not explicitly discuss the elastic recovery effect of the material and how it is governed as a function of strain rate. It is known that the strain rate

(strain rate = scratching speed/groove width) is positively correlated with scratching speed for a given groove width. To our best knowledge, few papers expounded on material elastic recovery in the grinding process. Also, it may be noted that much of the reported literature [10-14] in material spring back effect had been based on single grit scratch tests to quantify the elastic recovery of the workpiece whilst scratch experiments were usually carried out at lower speeds and presented a well-defined work-tool contact as opposed to the random grit-workpiece contact conditions during the ultra-fine grinding operation carried out at much higher speeds (strain rates).

Other reported papers [15-18] have attempted to measure the topography of the grinding wheel in terms of the distribution of grits (numbers and size). The reported measurement methods of grinding wheel topography can be divided into contact mode and non-contact mode categories [15]. As for contact methods, the topography of the workpiece is measured by moving the stylus probe across the lay direction with appropriate consideration of cut-offs and filters [19]. However, contact mode measurements are limited by the radius of the stylus making it hard to capture fine features of ultra-fine grits. Another drawback of contact mode measurement is that a stylus or probe might be caught by crevices when scanning below the outermost surface. Non-contact wheel measurement methods include 3D optical profilers and Scanning Electron Microscope (SEM) now known as image-based shape-from-shading (SFS) algorithm [20]. However, non-contact methods can only observe a limited section of the grinding wheel or would need a destructive preparation of wheel segment, which limits industrial-scale application.

Traditionally, scratch methods (although of a destructive nature) have been useful for understanding a topography as they produce a longitudinal isolated scratch which can

easily be analyzed using contact or non-contact mode measurement techniques. In the case of a rotational grinding operation which has a rotating wheel in its axis, a big challenge is to isolate the scratch during a single rotation of the wheel that is naturally overlapped by the subsequent grits. Solutions for avoiding the production of overlapped surface topography are proposed [21] in the past to obtain an isolated surface topography either (i) by moving the workpiece at a very fast speed compared to the wheel rotation speed or (ii) providing an angle of tilt while the wheel and workpiece are moved against each other. As one can imagine, while implementing the former approach, a compromise is made in operating at real machining speeds and an inherent speed-dependent influence would appear in the estimated results. The latter method of tilt angle isolated scratching exists but to our knowledge, this has not been applied in rotational grinding operations and this method is yet to be applied and assessed at the nanometric size scale. In the next section, details of customised experimental assembly are provided where the tilt angle approach method at the nanoscale was implemented to experimentally obtain the measure of elastic recovery in the silicon wafer. The new results reported here provide clarity that the grinding induced elastic recovery ratio (*EER*) is lower than that reported in the past from the grinding experiments assuming a single grit scratch test..

3. Experimental setup and methodology

A schematic diagram of the rotational grinding operation is shown in Fig. 2. As opposed to other grinding or milling operations, the degree of freedom of the grinding wheel in this operation are two (one rotation and one axial where pressure is applied) and this configuration in its original form does not allow the production of isolated scratches. It is hypothesised that by using a well-defined and structured sloped surface during the rotational grinding operation, leveraging the aforementioned tilt angle principle will be

aided. The novelty in the experiment here is that the rotational angular displacement of the wheel was controlled in such a manner that the isolated scratch lengths do not exceed the measurement range of an AFM (Atomic Force Microscope) to make all the measurements compliant to the AFM. Thus, this configuration helped in testing the tilt angle approach at the nanoscale by creating pre-defined scratch lengths and depths in the range of several tens of nanometers. The measurements were made along the length of the annular groove under the tapping mode until sufficient isolated scratches were recorded for subsequent analysis. It should be mentioned here that each residual scratch was assumed to represent a single grit in this study because tiny diamond grits are hardly broken to form multiple cutting edges which are a valid assumption taken into consideration in previous studies [22]. Therefore, the statistics of the numbers and heights of residual grooves represent those formed by the active grits.

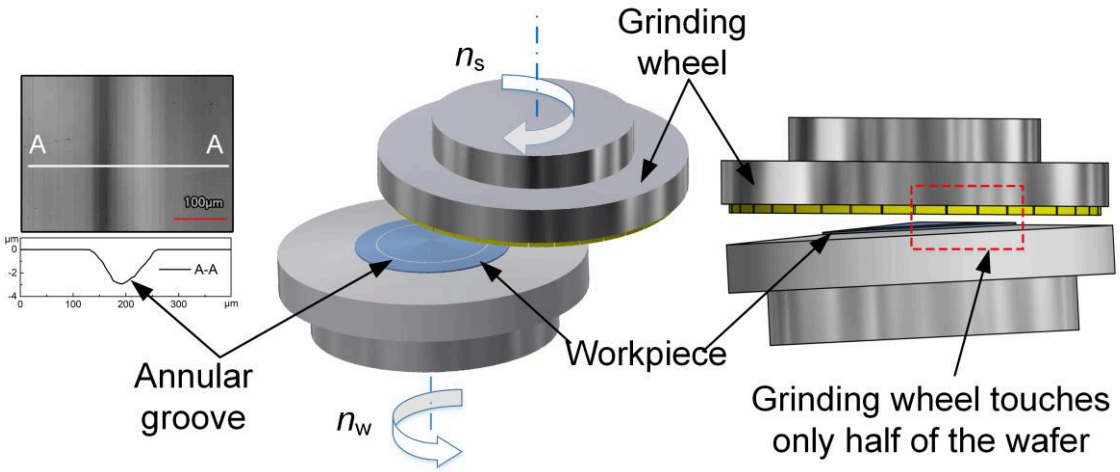

Fig. 2. Illustration of the scratch method based on rotational grinding. An annular groove was processed by polishing the (100) surface of Silicon before grinding with a highly protruded grit. The topography of isolated grinding scratches on the grooved surface provided detailed information about wheel topography and material response.

159 The grinding wheel used was a diamond cup wheel. Wafer grinding was carried out
160 after wheel dressing to ensure a stable working state of the grinding wheel and to avoid
161 the impact of grinding wheel dressing and wear on the experimental results. An annular
162 groove of diameter 75 mm was created by the polishing method on the surface of the
163 commercially available silicon (100) wafer of diameter 200 mm. The cross-sectional
164 profile (Section A-A) of this groove is shown in Fig. 2. An ultrafine grinding machine
165 (VG401 MK II, Okamoto, Japan) was employed to grind the sample surface with grinding
166 wheels of two mesh sizes, SD600 and SD3000 to ensure the robustness in the reported
167 results. Grinding wheels of these sizes are commonly used in the back-grinding of the
168 wafer thinning process. During the grinding process, both the wheel and the wafer rotated
169 around their axes, and the wheel was gently directed into the workpiece by moving it
170 along the axial direction at a prescribed velocity. The wafer elastically complies to the
171 curved shape presented by the chuck thus ensuring the grinding wheel touches only half
172 of the wafer shown in Fig. 2. More details about the grinding wheel and the process
173 parameters used are provided in Table 1. The selection of these parameters was primarily
174 governed by typical industrial practice to obtain elastic recovery of silicon under actual
175 grinding process. It is known that different parameters lead to a variation in the cutting
176 depth of the grits. In this study, the design of the sloped surface (polished groove) enables
177 observation of isolated scratches with gradually increased depth of cut. Therefore, the
178 variation of grit depth of cut due to varied parameters will not affect the practical value
179 of this experimental results.

180 An Atomic force microscope (XE-200, Park Systems, Korea) was used to measure the
181 isolated scratches under tapping mode. The nominal position detector noise of the AFM
182 used in this study was less than 0.1 nm and the measurement uncertainty was about 0.3

nm, much smaller than the characteristic size of the scratch. The measured length l of samples ground by wheel SD600 and SD3000 was 0.924 mm and 0.177 mm, respectively.

Table 1 Details of grinding wheel and process parameters

Mesh no.	Segment width, w (mm)	Wheel diameter (mm)	Rotational speed		Feed, f (μm/rpm)
			Wheel, n_w (rpm)	Wafer, n_s (rpm)	
SD600	3	350	2399	60	30/60=0.5
SD3000	3	350	2399	100	10/100=0.1

4. Results and discussions

4.1 Material's elastic recovery

Material's elastic recovery in the micromachining process refers to the tendency of the finished machined surface to recover elastically (spring back effect) after the tool has moved away. The material's elastic recovery ratio can be derived from isolated scratch topography. The interaction between an individual active grit tip and the workpiece is depicted in Fig. 3. Point A indicates where the active grit begins to interact with the workpiece. Constructed dashed line AB parallel to the ground surface through point A shows the programmed depth of cut revealing an ideal cutting tool path. Point C to Point D highlighted by a green area represents the extent of elastic recovery. The distance from point E to line AB represents the penetration depth h and point D to line AB represents the elastic recovery depth h_e, respectively. So in essence, h was the programmed depth of cut and experimentally one would obtain h-he as the measured depth of cut.

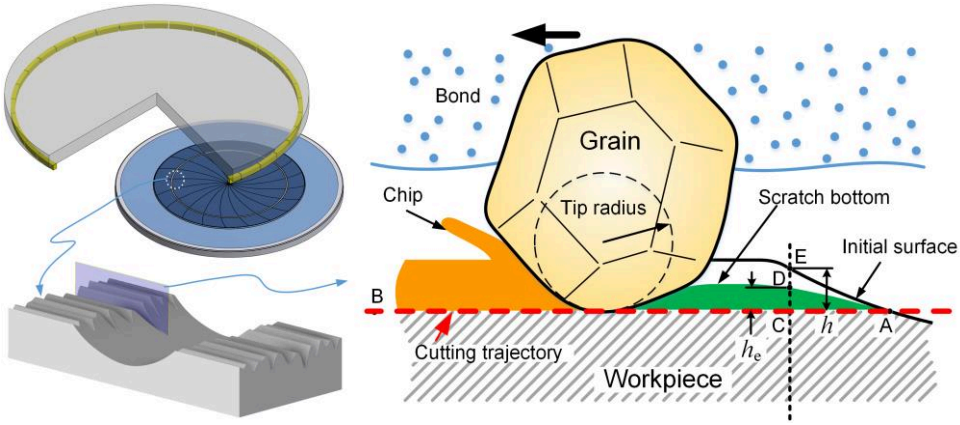

Fig. 3. A schematic illustration of scratch trajectory at a given instance chosen randomly on the inclined surface showing the cross-sectional view.

With the increase of the cutting depth, it is generally accepted that the deformation of hard, brittle materials will go through four phases, namely rubbing, plastic deformation, ploughing and cutting [23]. The cutting phase of brittle material includes ductile-regime cutting and brittle-regime cutting governed by the amount of depth of cut used. It should be mentioned that this study mainly focused on the ultra-fine grinding process where the ductile cutting was decisive in material removal due to the small depth of cut. The elastic recovery of material in the brittle regime cutting did not fall within the scope of this paper. For grits with large depth of cut, brittle fracture occurred on isolated scratches when the depth of cut exceeds a critical value. In this case, the measurement of scratch morphology was limited in the ductile-deformed region, i.e. the analysis and measurement of the scratch were terminated once brittle fracture occurred.

Determining the starting point of the measurement is a critical problem in the process of analyzing experimental data. It is difficult to obtain the penetration depth of active grits by the residual morphology of scratches due to the existence of the rubbing phase. However, in this study, a very interesting phenomenon was observed: a hillock-like protrusive nanostructure was produced at the beginning of each scratch and we find a

similar observation reported in Qian's work [24-25]. A sample structure measured by an AFM to highlight this hillock-like protrusive structure is shown in Fig.4.

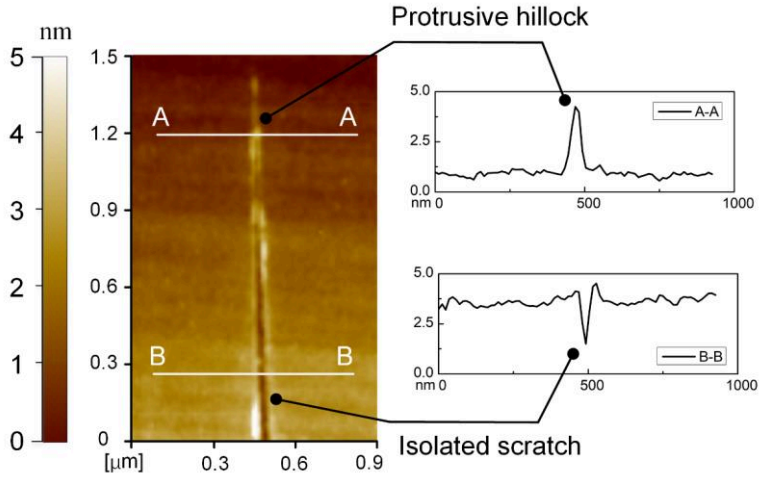

Fig. 4. A hillock-like protrusive nanostructure at the beginning of an isolated scratch measured by an AFM.

The previous study has demonstrated that these hillocks are induced by a combination of oxidation reaction and mechanical interaction and the critical contact stress σ for their formation was reported to be 11.1 GPa [24] – This is although a possible future area of research as to what conditions lead to the formation of these structures. The penetration depth of the grit at this point can be estimated by Hertzian theory [26]:

$$h_{\mathrm{cri}} = \frac{\pi^2 \sigma^2 R_{\mathrm{tip}}}{4E^2} \approx 0.019 R_{\mathrm{tip}} \tag{1}$$

where the reduced elastic modulus E for (100) silicon is about 126 GPa [27]. The tip radius R_{tip} was about one-tenth of the grit size, so the penetration depth of grits in the elastic-regime is only a few nanometers, which is much smaller than the maximum penetration depth-of-cut. Therefore, the position of the hillock is assumed to be the starting position of the interaction of the grits with the workpiece, i.e. the starting point A in Fig. 3.

One example of the results obtained for a single isolated scratch is shown in Fig. 5. Line X in Fig. 5(a) represents the height of an isolated scratch bottom, while line Y represents the height of the groove surface giving a slope of about 0.72º. Line Y (shown in 2D representation in Fig. 5(b)) represents the datum surface of the isolated scratch considering the continuity of the groove surface. Both lines are shown and plotted in Fig. 5(b). Fig. 5(b) shown in 2D was plotted by taking the bottom coordinate of the scratch profile in 3D thus considering the entire width and length of the isolated scratch. Therefore, the penetration depth h and the elastic recovery depth h_e is the difference between the datum surface (blue line) and scratched surface (red line) with respect to Point A shown in Fig. 5(b). It may be noted that the value of h_e varies at various points along the length of the scratch starting from Point A to Point F which represents an isolated scratch length. Beyond Point F, the scratch profile was overlapped by the other grits.

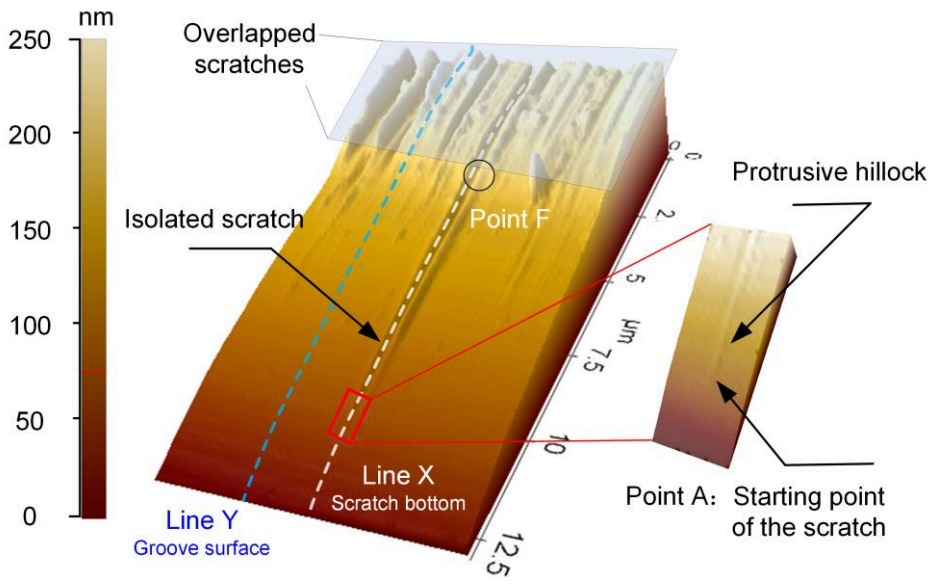

(a)

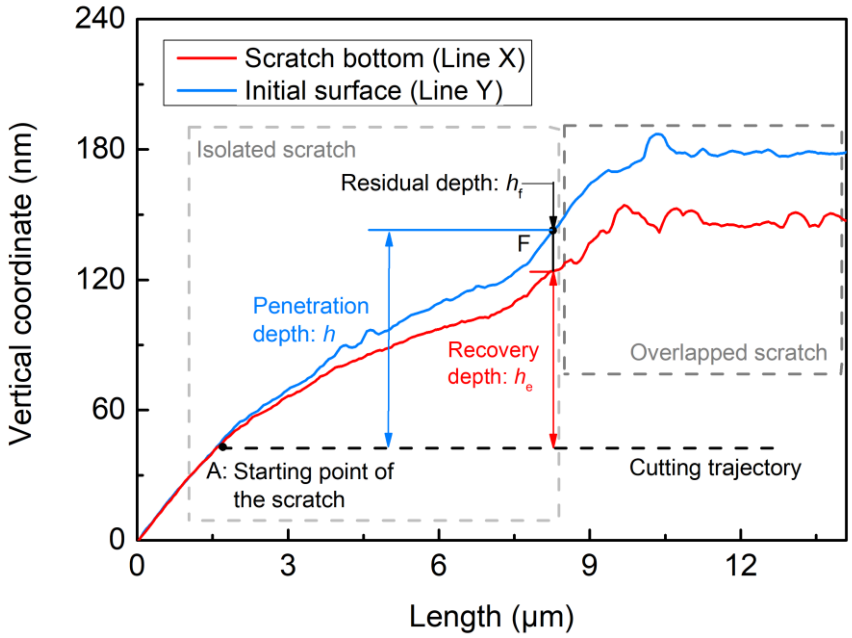

(b)

Fig. 5. An example of the residual depth h_f and penetration depth h obtained for a single isolated scratch. Point A in (a) shows a hillock-like protrusive nanostructure at the beginning of the scratch. Line X represents the height of an isolated scratch bottom, while line Y represents the height of the groove surface.

For statistical analysis, over 100 isolated scratches were analyzed for both types of wheels. The sampling area where these scratches were collected was randomly selected on the surface of the polished groove, then isolated scratches on the surface of the sampling area were analyzed one by one to ensure the results robustly and reproducible. To understand the influence of grit size, speed of scratch and influence of material properties on the depth of recovery (h_e), indentation theory proposed by Oliver and Pharr [27] was used to develop a semi-empirical analytical model. The recovery depth (h_e) and penetration depth (h) geometrically apply to the following equation:

$$h_f = h - h_e \tag{2}$$

where h_f is residual depth of an isolated scratch. For spherical tool tips, the resultant normal force P can be calculated from:

$$P = \alpha h_e^{\frac{3}{2}} = \alpha \left(h - h_f \right)^{\frac{3}{2}} \tag{3}$$

where α is a constant related to workpiece material and the grit size. Based on the results on high-speed nano-cutting tests [28], the resultant normal force P can also be written as a linear function of residual depth h_f:

$$P = kh_f \tag{4}$$

where coefficient k is a constant depending on cutting velocity. Comparing Eq. (3) and Eq. (4) gives:

$$kh_f = \alpha \left(h - h_f \right)^{\frac{3}{2}} \tag{5}$$

Adjustment of variables from Eq. (2) and (5) gives:

$$h = h_e + Ch_e^{\frac{3}{2}} \tag{6}$$

$$C = \frac{\alpha}{k} \tag{7}$$

where C is a strong function of α *(grit size dependence)* and k *(scratch speed dependence)*. In this work, the grit was approximated as being spherical, and the cutting speed was kept the same during the grinding process. Therefore, coefficient C for wheel SD3000 (typical average grit size ~ 5 μm) and SD600 (typical average grit size ~ 25.3 μm) at the same operational cutting speed (k being the same) was obtained as 0.0301 $nm^{-1/2}$ and 0.1004 $nm^{-1/2}$ respectively signifying that the increase in grit size leads to an increase in the value of C, as shown in Fig. 6(a) and Fig. 6(b). The fitted results were further used to evaluate the material elastic recovery ratio (*ERR*) during the grinding process:

290
$$ERR = \frac{\text{Recovery depth}\left(h_e\right)}{\text{Penetration depth}\left(h\right)} \tag{8}$$

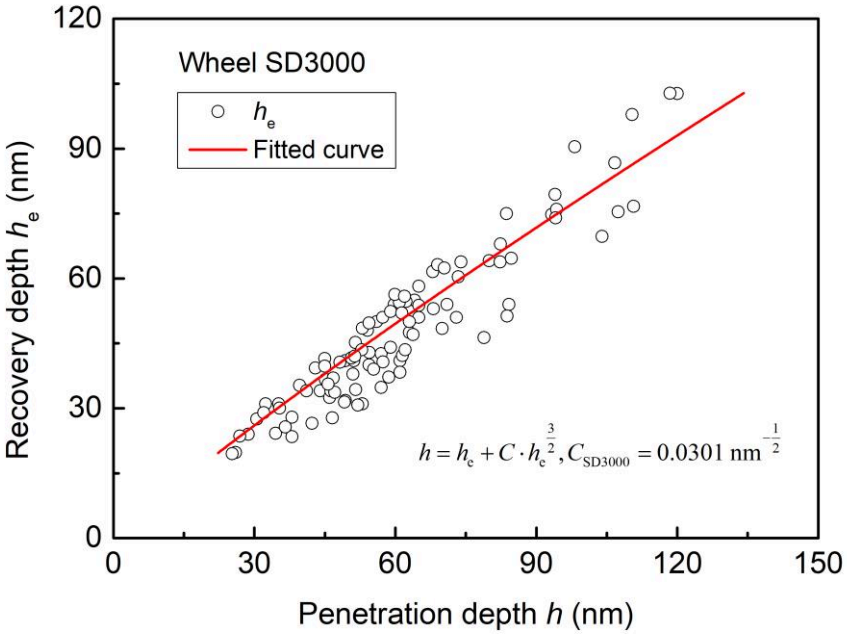

291
292 (a)

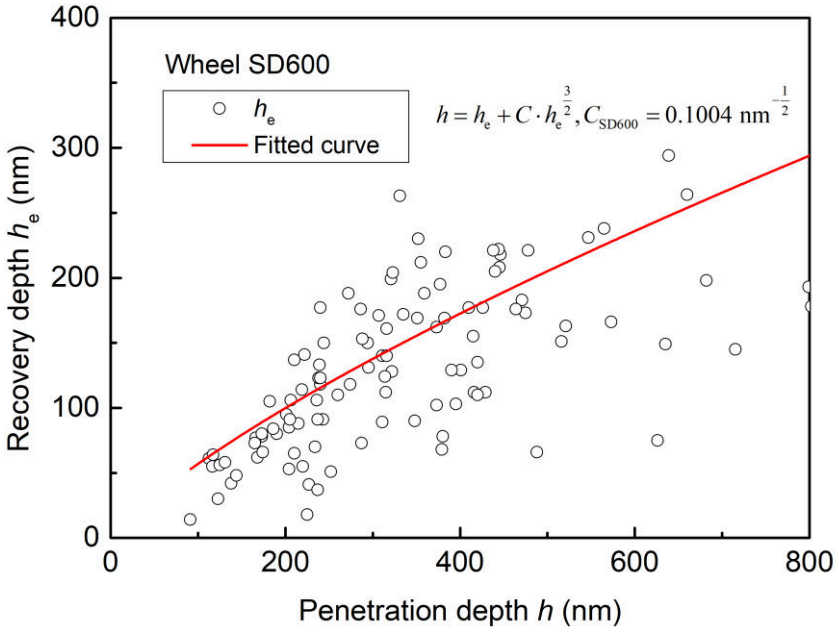

293
294 (b)

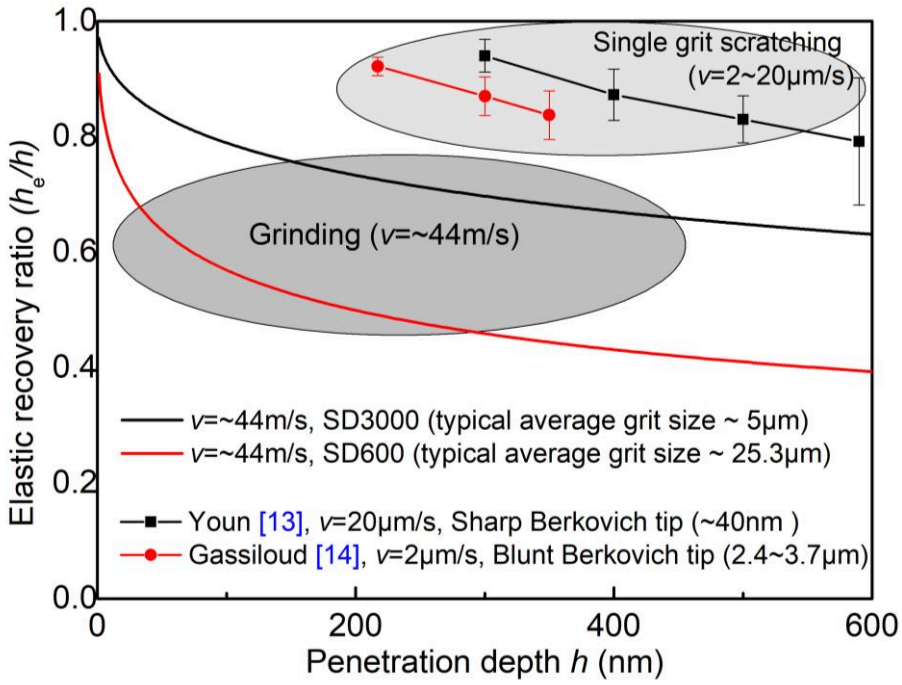

(c)

Fig. 6. Elastic recovery depth h_e as a function of penetration depth h for wheel size of (a) SD3000 and (b) SD600. Both plots were fitted by the semi-empirical model (Eq. (6)) and (c) Elastic recovery ratio (h_e/h) was plotted against penetration depth for both wheels.

The calculated *ERR* is plotted in Fig. 6(c) against the penetration depth. Due to the differences in the grit sizes, the *ERR* shown by the wheel SD3000 was larger than that of SD600 for the same penetration depth and the same scratch speed. At this point, it's worth comparing these results obtained by the grinding conditions with results obtained by the single grit scratch conditions, which was the motivation in pursuing this research study. The material elastic recovery of the (100) silicon during two reported single grit scratches carried out by Gassilloud [13] (scratch speed v = 2 μm/s, blunt Berkovich tip with estimated tip radius of 2.4~3.7 μm) and Youn [14] (scratch speed v = 20 μm/s, sharp Berkovich tip with an estimated tip radius of 40 nm) are compared in the plot Fig.6(c) with error bars indicating standard deviation. The previously reported scratch tests were

311 performed at low scratch velocities than an experimental grinding speed used in this study.
312 These results indicate that (i) smaller tip radius and lower cutting speed (low strain rate)
313 results in higher material elastic recovery for given penetration depth, and (ii) elastic
314 recovery of silicon would not change significantly unless the cutting speed or strain rate
315 changes more than one magnitude. In rotational grinding of silicon, the wheel speed is
316 the decisive factor that determines the speed of grits relative to the workpiece compared
317 to the workpiece speed. The wheel speed typically varies between 2000 rpm and
318 3500 rpm according to industrial practice. Therefore, the results of this study performed
319 at a wheel speed of 2400 rpm can serve as a reference for evaluating material recovery in
320 silicon grinding. The data of grinding group and single grit scratch group in Fig.6(c) also
321 shows that when cutting speed of grits is small, the size of the grit cutting tip is a crucial
322 factor influencing the amount of material elastic recovery for given penetration depth.
323 This helps explain why the fitting of SD 600 wheel in Fig. 6(b) is much worse than the
324 fitting of SD3000 in Fig.6(a) because the variation of grit tip size of SD600 is much larger
325 than that with wheel SD3000, which was discussed in the following section 4.2.
326 Following the aforementioned results, it is reasonable to infer that elastic recovery of the
327 material makes a significant influence on the form deviations (in the nm scales) and it is,
328 therefore, imperative to consider this aspect in developing the grinding models.

329 4.2 Grit tip radius

330 The previous sections were focused on obtaining the residual depth h_f and penetration
331 depth h by measuring an isolated scratch topography. This section describes the procedure
332 to obtain actively engaged grit tip radius. Fig. 7 shows a typical illustration of the
333 spherically shaped single grit engagement with the workpiece at a particular instance
334 adopted from the nanoindentation theory proposed by Oliver and Pharr [27].

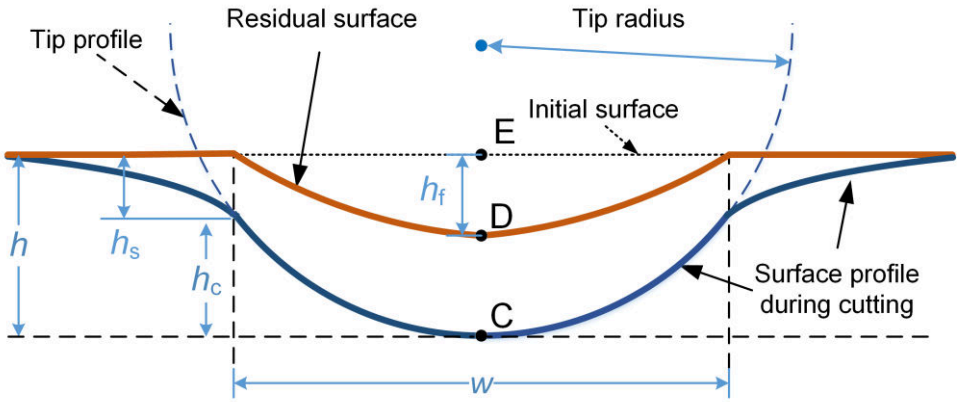

Fig. 7. A schematic illustration of a transverse cross-sectional view of residual isolated scratch. Points C, D, and E correspond to those in Fig. 3. Here h_c refers to contact depth, and h_s=h-h_c refers to vertical displacement at the contact perimeter. It is generally assumed that the contact width of the tool tip is equal to the residual width w of the groove [27, 29-30].

The contact depth h_c showed in Fig. 7 can be obtained by knowing the residual depth h_f and penetration depth h [27]:

$$h_s = \frac{\pi - 2}{\pi}\left(h - h_f\right) \tag{9}$$

$$h_c = h - h_s \tag{10}$$

where h_s is the vertical displacement at the contact perimeter. The contact depth h_c can accommodate the residual depth h_f and penetration depth h by substituting Eq. (9) into Eq. (10):

$$h_c = \frac{2}{\pi}h + \frac{\pi - 2}{\pi}h_f \tag{11}$$

It is generally assumed that the residual width w of the groove is equal to the contact width of the tool tip [27, 29-30]. Thus, the tip radius can be geometrically calculated as:

$$R_{tip} = \frac{h_c}{2} + \frac{w^2}{8h_c} \tag{12}$$

With Eq. (12), a statistical topography measurement of residual scratches can be used to evaluate the distribution of the tip radius. The calculation error of grit tip radius caused by the measurement error of penetration depth was estimated to be less than 5% according to Eq. (1) and Eq. (12). With this statistical data, the lognormal probability plot of the grit tip radius (scatter) is plotted in Fig. 8 against a theoretical lognormal distribution set (red line). The scatter points are close to the theoretical line which indicates that the grit tip radius can be well described by the lognormal distribution. Further calculations show that the natural logarithm of grit tip radius of wheel SD3000 and SD600 follows N (4.75, 0.666^2) and N (7.01, 0.817^2), respectively. The grit tip radius proves to be much smaller than the average grit radius. Hence, lognormal distribution of grit tip radius instead of average grit radius can be used when building models for the ultra-fine grinding process.

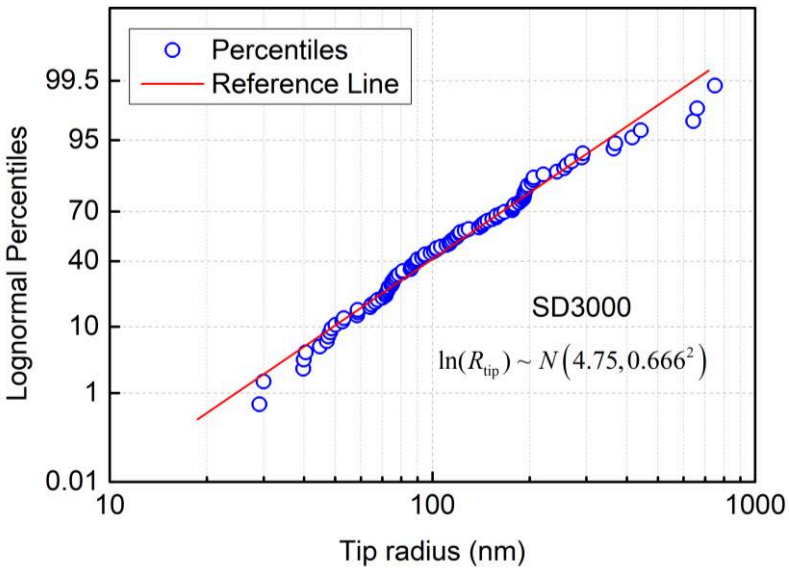

(a)

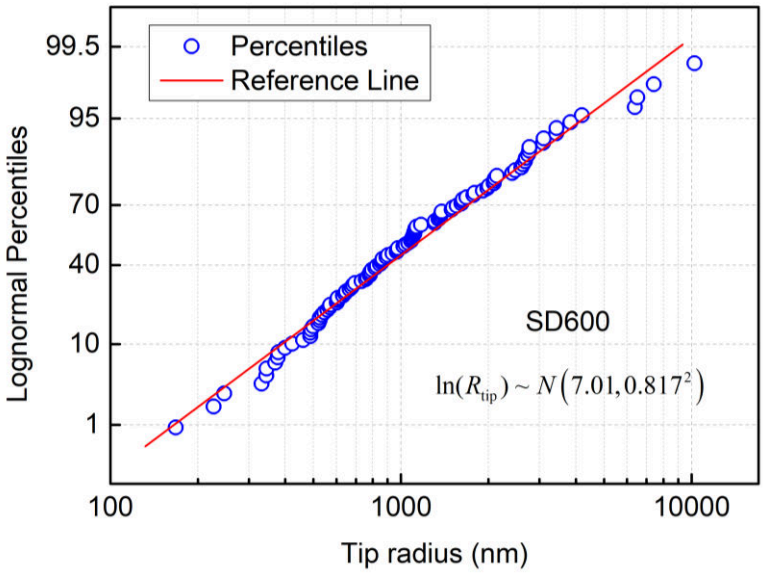

(b)

Fig. 8. Lognormal probability plot of the grit tip radius of wheel SD3000 (a) and SD600 (b). The experimental data set (scatter) is plotted against a theoretical lognormal distribution set (red line). The scatter points are close to the theoretical line which indicates that the grit tip radius can be well described by the lognormal distribution.

4. Conclusions

This paper provides a fresh experimental methodology to obtain the in-process measurement of material elastic recovery during the grinding process, hitherto not reported in the extant literature covering rotational grinding. Beside numerous findings that are reported within the paper, an active contribution this paper makes is to provide valuable experimental data of the extent of elastic recovery of monocrystalline silicon made during the experimental grinding conditions as opposed to previously reported single grit scratch tests which were only indicative but were not thorough enough to support modelling activities in this area. Based on the experimental results, a semi-empirical analytical model was developed, and the combined observations made from the analytical model and the experiments can be concluded as follows:

1. Isolated scratch trajectories are more relevant and meaningful than the overlapped scratch trajectories to infer and extract relevant data from the surface topography to study the problems in ultra-fine rotational grinding of monocrystalline silicon.
2. Elastic recovery depth (defined as h_e) was found to increase monotonically with the increase in penetration depth whilst the elastic recovery ratio (defined as h_e/h) decreases monotonically with increased penetration depth. These combined observations and comparison with single grit scratching tests pointed to the fact that the larger grit size and a coarser grinding wheel operated at a higher speed leads to a lesser extent of elastic recovery of silicon.
3. Much like the published literature on the topic of silicon nano-scratching, even during the precision grinding operation, hillock-like protrusive nanostructures were observed to form at the beginning of the scratch process and are an interesting area of exploration for future research.
4. The grit tip radius was found to follow a lognormal distribution and it turns out that the active grit tip radius is much smaller than the average grit radius. Hence, lognormal distribution of grit tip radius instead of average grit radius is a more appropriate measure while building suitable models of the ultra-fine rotational grinding process.

Acknowledgments

All authors appreciate the financial support from the National Natural Science Foundation of China (51875078, 51991373, 51975094), and the Science Fund for Creative Research Groups of NSFC of China (51621064). The cross-exchange became possible due to the financial support provided by the UKRI to SG via Grants No.: (EP/K503241/1, EP/L016567/1, EP/S013652/1, EP/T001100/1, EP/S036180/1 and

EP/T024607/1). Part of this work used Isambard Bristol, UK supercomputing service accessed by the Resource Allocation Panel (RAP) grant. SG is particularly grateful to the fantastic financial support provided by H2020 (Cost Actions (CA15102, CA18125, CA18224 and CA16235)), EURAMET EMPIR A185 (2018), Royal Academy of Engineering (Grant No. IAPP18-19\295- Indo-UK partnership and Grant No. TSP1332 - South Africa- UK partnership) and Newton Fellowship award from the Royal Society (NIF\R1\191571).

References

[1] Goel S, Kovalchenko A, Stukowski A, Cross G. Influence of microstructure on the cutting behaviour of silicon. Acta Mater., 2016, 105, 464-478.

[2] International Technology Roadmap for Semiconductors. http://www.itrs.net (2015)

[3] Brinksmeier E, Mutlugünes Y, Klocke F, Aurich J C, Shore P, Ohmori H. Ultra-precision grinding. CIRP Ann. Manuf. Technol., 2010, 59(2), 652-671.

[4] Goel S, Luo X, Comley P, Reuben R L, Cox A. Brittle–ductile transition during diamond turning of single crystal silicon carbide. Int. J. Mach. Tools Manuf., 2013, 65: 15-21.

[5] Goel S, Luo X, Agrawal A, Reuben R L. Diamond machining of silicon: a review of advances in molecular dynamics simulation. Int. J. Mach. Tools Manuf., 2015, 88: 131-164.

[6] Young H T, Liao H T, Huang H Y. Novel method to investigate the critical depth of cut of ground silicon wafer. J. Mater. Process. Technol., 2007, 182(1-3): 157-162.

[7] Lin B, Zhou P, Wang Z G, Yan Y, Kang R K, Guo D M. Analytical Elastic–Plastic Cutting Model for Predicting Grain Depth-of-Cut in Ultrafine Grinding of Silicon Wafer. J. Manuf. Sci. Eng.-Trans. ASME, 2018, 140(12): 121001.

[8] Zhou L, Tian Y B, Huang H, Sato H, Shimizu J. A study on the diamond grinding of ultra-thin silicon wafers. Proc. Inst. Mech. Eng. Part B-J. Eng. Manuf., 2012, 226(1): 66-75.

[9] Pei Z J, Strasbaugh A. Fine grinding of silicon wafers. Int. J. Mach. Tools Manuf., 2001, 41(5): 659-672.

[10] Ge M, Zhu H, Huang C, Liu A, Bi W. Investigation on critical crack-free cutting depth for single crystal silicon slicing with fixed abrasive wire saw based on the scratching machining experiments. Mat. Sci. Semicon. Proc., 2018, 74: 261-266.

[11] Aurich J C, Steffes M. Single grain scratch tests to determine elastic and plastic material behavior in grinding. Advanced Materials Research. Trans Tech Publications Ltd, 2011, 325: 48-53.

[12] Öpöz T T, Chen X. Experimental investigation of material removal mechanism in single grit grinding. Int. J. Mach. Tools Manuf., 2012, 63: 32-40.

[13] Gassilloud R, Ballif C, Gasser P, Buerki G, Michler J. Deformation mechanisms of silicon during nanoscratching. Phys. Status Solidi A-Appl. Res., 2005, 202(15): 2858-2869.

[14] Youn S W, Kang C G. A study of nanoscratch experiments of the silicon and borosilicate in air. Mat. Sci. Eng. A-Struct., 2004, 384(1-2): 275-283.

[15] McDonald A, Bauer R, Warkentin A. Design and validation of a grinding wheel optical scanner system to repeatedly measure and characterize wheel surface topography. Measurement, 2016, 93: 541-551.

[16] Ye R, Jiang X, Blunt L, Cui C, Yu Q. The application of 3D-motif analysis to characterize diamond grinding wheel topography. Measurement, 2016, 77: 73-79.

[17] Tahvilian A M, Liu Z, Champliaud H, Hazel B, Lagacé M. Characterization of grinding wheel grain topography under different robotic grinding conditions using confocal microscope. Int. J. Adv. Manuf. Tech., 2015, 80(5-8): 1159-1171.

[18] Darafon A, Warkentin A, Bauer R. Characterization of grinding wheel topography using a white chromatic sensor. Int. J. Mach. Tools Manuf., 2013, 70: 22-31.

[19] Leach R K. Measurement Good Practice Guide No. 37, The measurement of surface texture using stylus instruments. National Physical Laboratory, Ed, 2001.

[20] Wang J, Su R, Leach R, Lu W, Zhou L, Jiang X. Resolution enhancement for topography measurement of high-dynamic-range surfaces via image fusion. Opt. Express, 2018, 26(26): 34805-34819.

[21] Malkin Stephen, Changsheng Guo. Grinding technology: theory and application of machining with abrasives. Industrial Press Inc., 2008.

[22] Zhou L, Ebina Y, Wu K, Shimizu J, Onuki T, Ojima H. Theoretical analysis on effects of grain size variation. Precis. Eng., 2017, 50: 27-31.

[23] Zhang Z, Yan J, Kuriyagawa T. Study on tool wear characteristics in diamond turning of reaction-bonded silicon carbide. Int. J. Adv. Manuf. Tech., 2011, 57(1-4): 117-125.

[24] Yu B, Dong H, Qian L, Chen Y, Yu J, Zhou Z. Friction-induced nanofabrication on monocrystalline silicon. Nanotechnology, 2009, 20(46): 465303.

[25] Yu B, Li X, Dong H, Chen Y, Qian L, Zhou Z. Towards a deeper understanding of the formation of friction-induced hillocks on monocrystalline silicon. J. Phys. D Appl. Phys., 2012, 45(14): 145301.

[26] Johnson K L. Contact mechanics. Cambridge university press, 1987.

[27] Oliver W C, Pharr G M. An improved technique for determining hardness and elastic modulus using load and displacement sensing indentation experiments. J. Mater. Res., 1992, 7(6): 1564-1583.

[28] Huang N, Yan Y, Zhou P, Kang R, Guo D. Elastic-plastic deformation of single-crystal silicon in nano-cutting by a single tip tool. Jpn. J. Appl. Phys, 2019.

[29] Jing X, Maiti S, Subhash G. A new analytical model for estimation of scratch - induced damage in brittle solids. J. Am. Ceram. Soc., 2007, 90(3): 885-892.

[30] Kaupp G. Atomic force microscopy, scanning nearfield optical microscopy and nanoscratching: application to rough and natural surfaces. Springer Science & Business Media, 2006.

Elastic recovery of monocrystalline silicon during ultra-fine rotational grinding

Huang, Ning

2020-05-21

Huang N, Yan Y, Zhou P, et al., (2020) Elastic recovery of monocrystalline silicon during ultra-fine rotational grinding. Precision Engineering, Volume 65, September 2020, pp. 64-71
https://doi.org/10.1016/j.precisioneng.2020.05.004